Real-time x-ray fluoroscopy-based catheter detection and tracking for cardiac electrophysiology interventions

Ma, Y., Gogin, N., Cathier, P., Housden, R. J., Gijsbers, G., Cooklin, M., O'Neill, M., Gill, J., Rinaldi, C. A., Razavi, R. & Rhode, K.

Original citation:
Ma, Y, Gogin, N, Cathier, P, Housden, RJ, Gijsbers, G, Cooklin, M, O'Neill, M, Gill, J, Rinaldi, CA, Razavi, R & Rhode, K 2013, 'Real-time x-ray fluoroscopy-based catheter detection and tracking for cardiac electrophysiology interventions', Medical Physics, vol. 40, no. 7, 071902.
https://dx.doi.org/10.1118/1.4808114

DOI 10.1118/1.4808114
ISSN 0094-2405
ESSN 2473-4209

Publisher: Wiley

Real-time x-ray fluoroscopy-based catheter detection and tracking for cardiac electrophysiology interventions

YingLiang Ma[a)]
Division of Imaging Sciences and Biomedical Engineering, King's College London, London SE1 7EH, United Kingdom

Nicolas Gogin and Pascal Cathier
Medisys Research Group, Philips Healthcare, Paris 92156, France

R. James Housden
Division of Imaging Sciences and Biomedical Engineering, King's College London, London SE1 7EH, United Kingdom

Geert Gijsbers
Interventional X-ray, Philips Healthcare, Best 5680 DA, The Netherlands

Michael Cooklin, Mark O'Neill, Jaswinder Gill, and C. Aldo Rinaldi
Department of Cardiology, Guys and St. Thomas' Hospitals NHS Foundation Trust, London SE1 7EH, United Kingdom

Reza Razavi and Kawal S. Rhode
Division of Imaging Sciences and Biomedical Engineering, King's College London, London SE1 7EH, United Kingdom

(Received 10 October 2012; revised 30 April 2013; accepted for publication 3 May 2013; published 11 June 2013)

Purpose: X-ray fluoroscopically guided cardiac electrophysiology (EP) procedures are commonly carried out to treat patients with arrhythmias. X-ray images have poor soft tissue contrast and, for this reason, overlay of a three-dimensional (3D) roadmap derived from preprocedural volumetric images can be used to add anatomical information. It is useful to know the position of the catheter electrodes relative to the cardiac anatomy, for example, to record ablation therapy locations during atrial fibrillation therapy. Also, the electrode positions of the coronary sinus (CS) catheter or lasso catheter can be used for road map motion correction.
Methods: In this paper, the authors present a novel unified computational framework for image-based catheter detection and tracking without any user interaction. The proposed framework includes fast blob detection, shape-constrained searching and model-based detection. In addition, catheter tracking methods were designed based on the customized catheter models input from the detection method. Three real-time detection and tracking methods are derived from the computational framework to detect or track the three most common types of catheters in EP procedures: the ablation catheter, the CS catheter, and the lasso catheter. Since the proposed methods use the same blob detection method to extract key information from x-ray images, the ablation, CS, and lasso catheters can be detected and tracked simultaneously in real-time.
Results: The catheter detection methods were tested on 105 different clinical fluoroscopy sequences taken from 31 clinical procedures. Two-dimensional (2D) detection errors of 0.50 ± 0.29, 0.92 ± 0.61, and 0.63 ± 0.45 mm as well as success rates of 99.4%, 97.2%, and 88.9% were achieved for the CS catheter, ablation catheter, and lasso catheter, respectively. With the tracking method, accuracies were increased to 0.45 ± 0.28, 0.64 ± 0.37, and 0.53 ± 0.38 mm and success rates increased to 100%, 99.2%, and 96.5% for the CS, ablation, and lasso catheters, respectively. Subjective clinical evaluation by three experienced electrophysiologists showed that the detection and tracking results were clinically acceptable.
Conclusions: The proposed detection and tracking methods are automatic and can detect and track CS, ablation, and lasso catheters simultaneously and in real-time. The accuracy of the proposed methods is sub-mm and the methods are robust toward low-dose x-ray fluoroscopic images, which are mainly used during EP procedures to maintain low radiation dose. [http://dx.doi.org/10.1118/1.4808114]

Key words: catheter detection, catheter tracking, cardiac electrophysiology

I. INTRODUCTION

X-ray fluoroscopically-guided cardiac electrophysiology (EP) interventions are routinely carried out for diagnosis and treatment of cardiac arrhythmias. X-ray images have poor soft tissue contrast and, for this reason, overlay of static three-dimensional (3D) roadmaps can be used to add anatomical information. The roadmaps can be derived from preprocedural computed tomography (CT) images,[1–3] magnetic resonance images (MRI),[4] or C-arm CT and rotational x-ray angiography (RXA) images.[5–7] Further combining the pre-procedural image with electro-anatomical mapping systems can provide detailed anatomical information. Anatomical information from live 3D echo can also be combined with x-ray fluoroscopy for navigational purposes.[8,9] A review of these image fusion techniques can be found in Ref. 10. Many different types of catheters are used during EP procedures, each having specific configurations of radio-opaque markers or electrodes [see Fig. 1(b)]. These electrodes are used for the measurement of electrical signals within the heart and also for the delivery of radio frequency energy during ablation treatments.[11] Accurate and robust localization of catheters in the x-ray images can provide enhanced functionality during procedures for guidance and also for postprocedural analysis.

One of the important clinical applications for the localization of catheters is to correct for respiratory motion. Currently, a major limitation of 3D road mapping technologies is that the overlay image remains static and does not move with the patients respiratory motion. In some cases, respiratory motion can cause a two-dimensional (2D) registration error of over 14 mm.[12] Respiratory motion correction can be achieved by using the motion of lasso[13,14] or coronary sinus (CS) (Refs. 15–17) catheter, when the lasso or CS catheter remain fixed with respect to the cardiac anatomy and only move with the respiratory and cardiac motions. Another important application of catheter localization is to record the position of the ablation catheter tip and map it onto the 3D roadmap during ablation therapies.[18]

The 3D catheter path can be reconstructed from two x-ray views using the methods in Refs. 19 and 20. Alternatively, the 3D position of the ablation catheter tip can be automatically calculated by using synchronously acquired biplane images from a biplane x-ray system. However, a biplane system is less common than a monoplane system due to its much higher cost, and involves increased radiation exposure for both the patient and the clinician.[13] In order to generate biplane x-ray images from a monoplane x-ray system, motion gating methods can be used to match a pair of images with similar respiratory and cardiac phases from two image sequences that are sequentially acquired from different angles. One method for automatic image-based motion gating is to calculate the cumulated phase shift in the spectral domain from x-ray fluoroscopic image sequences.[21] This method is based on detection of the energy change in the images. As the method uses the overall motion of moving objects, the cardiac and respiratory cycle motions detected by this method could be erroneous when the clinician manipulates the catheters or injects contrast agent. Therefore, a motion gating method based on catheter motion detection would be potentially more accurate and robust.

All of these applications require fast, accurate, and robust image-based catheter detection methods. However, to design such methods and use them during EP procedures is a challenging task. The speed of the detection method should be real-time (at least 10 fps). The region of interest should cover the whole x-ray fluoroscopic image since the catheters can be moved very quickly and large, sudden respiratory motion can also cause large, sudden movement of the catheters. Therefore, catheter detection and tracking methods on the whole x-ray image should be used instead of using small regions of interest. Finally, the detection methods have to be robust enough to be used routinely during clinical procedures. A technique for tracking the ablation catheter in x-ray images was first proposed by Franken *et al.*[22] The computational cost was relatively high and implementation on a graphical processing unit (GPU) was suggested. Weide *et al.*[23] developed a more efficient method for tracking intravascular devices in interventional MR images based on tracking paramagnetic markers. The computation for a single image by their method took 0.3 s. Schenderlein *et al.*[24] proposed a catheter tracking method using snakes (active contour models).

More recently, Brost *et al.*[13,14] developed a model-based lasso catheter tracking algorithm and achieved a maximum frame rate of 3 fps in a biplane x-ray system (10 fps in a monoplane x-ray system). However, the tracking method required manual initialization. Wu *et al.*[25] proposed a learning based approach to temporally track and detect catheter electrodes in fluoroscopy sequences. This approach achieved 0.50 mm median error and 0.76 mm mean error for CS catheter tracking and 97.8% of evaluated data had errors less than 2.00 mm. A tracking speed of 5 fps was achieved on most data. Yatziv *et al.*[26] presented a catheter detection method based on cascade classifiers. Although their method achieved 10 fps and a 3.97% detection failure rate, it only detected the catheter tip electrode and could fail when a thicker lasso catheter was present.

We have previously developed a detection method for ten-electrode CS catheters based on blob detection.[15–17] This method was limited to one type of catheter, was not robust to occluded electrodes and required the catheter tip to be in view. In this paper, we extend our basic detection method with novel contributions that include (1) a unified framework that can be adapted to detect any of the three most common types of EP catheter (CS, ablation and lasso); (2) a method to track these catheters based on custom templates derived from the detection, which provides robust tracking even when some electrodes are overlapped with other radiographically dense objects or are outside the field of view; and (3) real-time fully-automated operation with simultaneous discrimination of all three catheter types. The developed methods were validated using a large cohort of clinical data using quantitative error metrics and also subjective evaluation by experienced clinicians for clinical utility.

In Secs. II–IV, the proposed catheter detection and tracking algorithms are presented in Sec. II. The evaluation of both

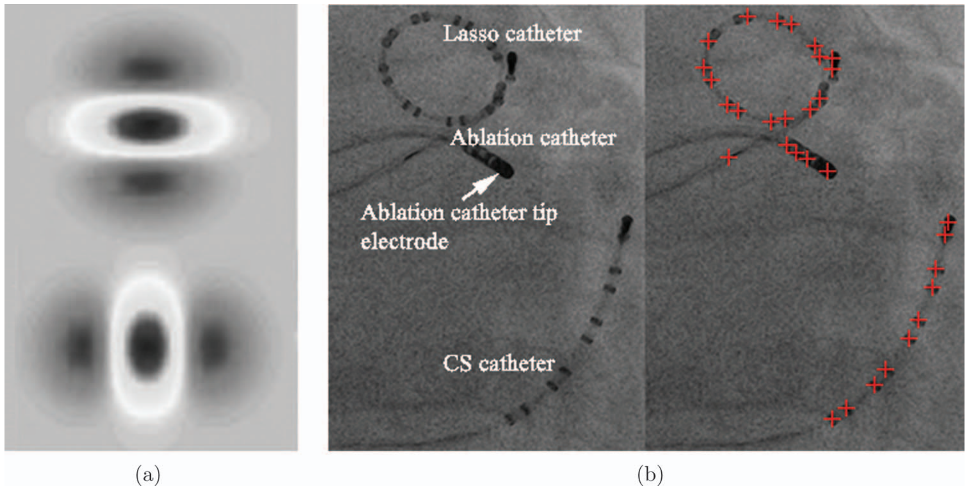

FIG. 1. (a) Gaussian derivative masks. (b) Example of the result of the blob detection method in a low dose X-ray image. The crosses are the positions of electrode-like blobs.

methods is given in Sec. III. Finally, a conclusion and brief discussion is given in Sec. IV.

II. METHODS

Cardiac EP catheters comprise a smooth and flexible tube with several metal electrodes in the tip region and are designed to be highly visible in normal or low dose x-ray fluoroscopic images. The common features of catheters are a larger metal electrode at the tip of the catheter and several equal-size metal electrodes proximal to this. On the other hand, different types of EP catheter have different unique features, which can be used to discriminate them from each other. Our novel generalized computational framework for catheter detection and tracking includes fast blob detection, shape-constrained searching, model-based detection, and template-based tracking as described in Secs. II.A–II.D.

II.A. Blob detection

Electrode-like objects were detected using a fast blob detector based on the determinant of the Hessian matrix,[27,28] which is defined as

$$\det\mathrm{H}(L(x, y; t_0)) = L_{xx}L_{yy} - L_{xy}^2, \tag{1}$$

where $L(x, y; t) = I(x, y) * g(x, y; t)$ is the scale-space representation of the image $I(x, y)$ with the scale factor t and $g(x, y; t)$ is a Gaussian filter. In practice, the determinant is calculated directly via L_{xx}, L_{yy} and L_{xy} using directional Gaussian derivative filters applied to the original image, e.g., $L_{xx} = I(x, y) * g_{xx}$, where

$$g_{xx}(x, y; t_0) = -\frac{1}{2\pi t_0^2}\left(1 - \frac{x^2}{t_0}\right) e^{-(x^2+y^2)/2t_0}. \tag{2}$$

Figure 1(a) shows the precomputed Gaussian derivative masks.

Blobs are detected as regional maxima of the determinant of the Hessian matrix and the strength of the blob is defined as

$$\mathrm{Blob} = t_0 \det\mathrm{H}(L(x, y; t_0)). \tag{3}$$

From Eq. (3), it is known that the strength of the blob is dependent on the scale factor and the choice of scale factor determines the size of electrode that is detected. A method is required that simultaneously detects the differently sized electrodes on the CS, ablation and lasso catheters. As the size of the lasso catheter electrodes is very similar to the size of the CS catheter electrodes, four fixed scale factors are used to detect the tip and proximal electrodes on the three types of catheter. The scale factor is $t_0 = \sigma^2$ (σ is the standard deviation of the Gaussian function) as the border of the blob is likely to occur at the maximum slope of the Gaussian function. Figure 1(b) demonstrates the result of blob detection in a low-dose x-ray image. The value of the blob size s ($s = \sigma$) was set to 8 pixels for the CS catheter tip electrode and 4 pixels for the smaller electrodes. For the ablation catheter, s was set to 16 or 6 pixels for the tip electrode and the smaller electrodes, respectively. The pixel sizes of the electrodes were calculated from their physical size (mm) and the conversion took account of the magnification factor of the x-ray system. The magnification factor was estimated using $M = D_{\mathrm{det}} D_{\mathrm{pat}}$, where D_{det} is the distance from the x-ray source to the detector and D_{pat} is the distance from the source to the patient. The conversion factor from mm to image pixels was then MR_{det} where R_{det} is the constant pixel size on the detector.

In addition, the first and second eigenvectors of the Hessian matrix were computed based on the region covered by the blobs. The first eigenvector corresponds to the orientation of blobs and the second eigenvector is the vector perpendicular to the first eigenvector.

II.B. Shape constrained searching

First, the 50 highest strength blobs are selected from the blob detection method and they are sorted by strength from strongest to weakest. The blob strength is correlated with the blob size, s, since from Eq. (3), we know that the strength of the blob is dependent on the scale factor t. Therefore, the larger catheter electrodes are likely to have stronger blobs. The number 50 was empirically determined and relates to

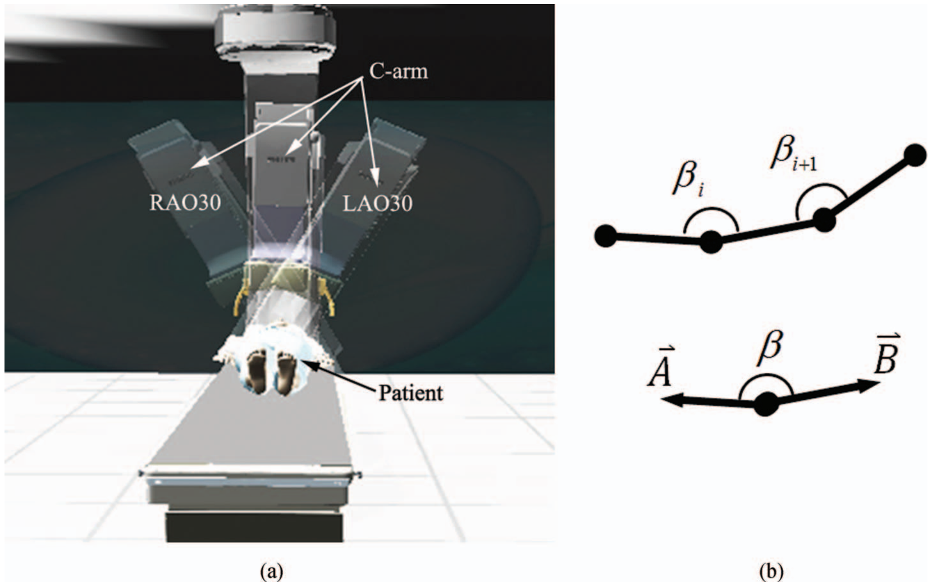

FIG. 2. (a) Illustrations of the rotation of the C-arm at left/right anterior oblique 30°, viewed from a patients foot end. (b) The definition of folding angle β.

the number of blob-like structures typically detected in x-ray data, the majority of which correspond to the electrodes of catheters. Of the three catheters used in a typical EP procedure, a CS catheter has 4–10 electrodes, an ablation catheter has 4 electrodes and a lasso catheter has 10–20 electrodes. Therefore 50 is a reasonable number. Following blob detection, a shape constrained search algorithm is used to identify which combination of blobs represents an EP catheter.

II.B.1. Smooth curve based search algorithm

For detecting a flexible catheter, e.g., a CS catheter or defibrillation catheter, a smooth curve based search algorithm is used. The search algorithm starts with the first 10 of the 50 strongest blobs from the blob detection algorithm and uses them as candidates for the catheter tip electrode. Since there are typically three catheters used in an EP procedure, the tip electrodes for all catheters are likely to be included in the first ten strongest blobs.

From the position of each candidate tip electrode, the smooth curve based search algorithm finds the nearest blob which satisfies two conditions. First is the maximum electrode gap (5 mm, or 20 pixels in a 512 × 512 pixel image). This is twice the length of the maximum distance between two neighboring catheter electrodes, which also takes account of variations from different catheter manufacturers. The second condition is the folding angle β, which should be larger than 90°, as catheters in human vessels are likely to be in a smooth curve shape when the catheter is projected onto the 2D x-ray image within the range of normal clinical C-arm angles. The EP procedures usually use C-arm angles from LAO 30 to RAO 30 [illustrated in Fig. 2(a)]. The folding angle measures how sharply a curved catheter has turned and is illustrated in Fig. 2(b). As the folding angle β must be larger than 90°, this can be translated into $\overrightarrow{A} \cdot \overrightarrow{B} < 0$. Using these two conditions, the search algorithm is likely to find blobs along a smoothly curved path. It will stop when all electrodes are found or no more blobs are within the range of maximum electrode gap.

II.B.2. Line based search algorithm

The line based search algorithm assumes that the catheter is very rigid in the region of the electrodes. The ablation catheter is a good example as the region of the catheter tip and its other three electrodes is very rigid [see Fig. 3(a)] and

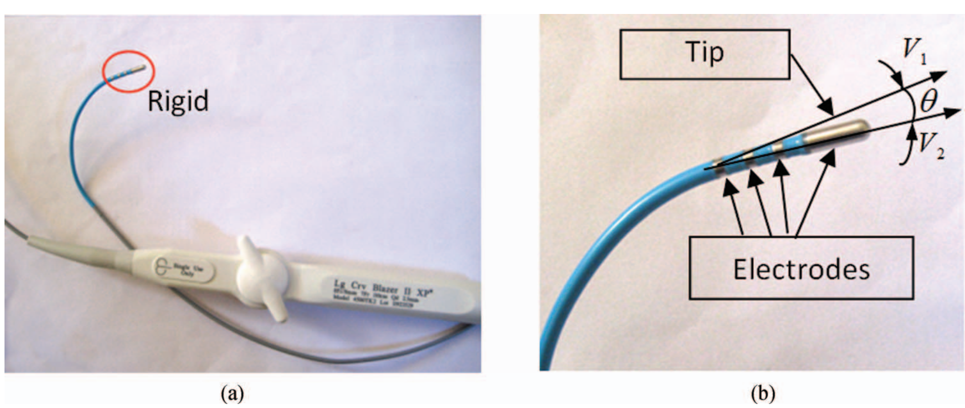

FIG. 3. (a) Ablation catheter. The rigid area is within the circle. (b) The definition of the turning angle.

cannot make a turning angle of more than 30°. The turning angle θ is defined as the angle between the direction vector of the last two electrodes, V_1, and the orientation vector of the catheter tip electrode, V_2 [see Fig. 3(b)]. As the catheter tip electrode is a large and solid metal electrode, it is again expected to be one of the first ten strongest blobs. From the ten candidates, the line based search algorithm searches for the other electrodes along the direction and the opposite direction of the blob orientation vector which is the first eigenvector of the Hessian matrix. The reason for searching in two directions is because of the symmetry of the catheter tip, which means that the orientation vector calculated from the blob detection is not always from the distal end to the proximal end of the catheter. Two constraints are applied to the search: the maximum gap between electrodes and the turning angle θ. The θ condition can be written as

$$\cos\theta = \frac{\overrightarrow{V_1} \cdot \overrightarrow{V_2}}{\overrightarrow{V_1} \quad \overrightarrow{V_2}} > \cos\alpha, \tag{4}$$

where α is the maximum turning angle for the ablation catheter, in this case 30°.

For the ablation catheter, there is some variation in the maximum electrode gap from several manufacturers. We chose the maximum (5 mm) among them with a cutoff threshold of twice that value (10 mm or 40 pixels based on a pixel to mm ratio of 0.25). The search algorithm iteratively searches for blobs which satisfy these two constraints until the maximum number of blobs is reached. This may be more than the maximum number of electrodes (four for the ablation catheter), as other electrode-like objects could also be detected.

II.B.3. Ellipse based search algorithm

The ellipse based search algorithm is used to detect circular or elliptical shaped catheters, such as the lasso catheter. Similar to the first two methods, the search algorithm starts with the first ten strongest blobs. As all circular or elliptical shaped catheters are deformed from smooth line catheters [see Fig. 4(a)], the nearby second electrode is expected to be found along the orientation direction of the catheter tip electrode, computed as the first eigenvector of the Hessian matrix. Therefore the second electrode is found using a line based search algorithm in this direction.

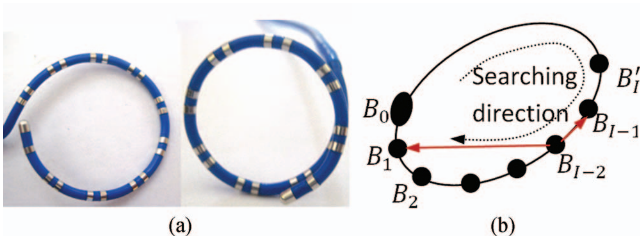

FIG. 4. (a) The circular lasso catheter is formed from a smooth line catheter. (b) The definition of reference centripetal direction vector $\overrightarrow{C}_0 = \overrightarrow{B_{I-2}B_1} \times \overrightarrow{B_{I-2}B_{I-1}}$. B_0 is the position of the catheter tip which is excluded from the calculation because it is sometimes located outside the ellipse or circle. B_I is the position of a candidate blob.

To collect and compute some basic geometric information about the shape of the catheter, the next three electrodes are detected using only the nearest blob with the maximum gap constraint. After these electrodes are successfully detected, the centripetal direction vector can be computed, which tells the search algorithm whether the rest of the electrodes are in a clockwise or anti-clockwise direction. As shown in Fig. 4(b), the reference centripetal direction vector $\overrightarrow{C_0}$ is computed using the positions of existing blobs

$$\overrightarrow{C_0} = \overrightarrow{B_{I-2}B_1} \times \overrightarrow{B_{I-2}B_{I-1}}, \tag{5}$$

where $\times$ is the cross product operator and I is the index of the blob. The current centripetal direction vector is

$$\overrightarrow{C_I} = \overrightarrow{B_{I-1}B_{I-2}} \times \overrightarrow{B_{I-1}B_I}, \tag{6}$$

where B_I is the position of a candidate blob. To test whether $\overrightarrow{C_0}$ and $\overrightarrow{C_I}$ are in the same direction, a dot product $\overrightarrow{C_0} \cdot \overrightarrow{C_I}$ is used, with $\overrightarrow{C_0} \cdot \overrightarrow{C_I} > 0$ indicating the same direction. The search algorithm iteratively searches for blobs which satisfy the maximum gap and centripetal direction constraints until the number of electrodes on the catheter (20 in this case) is reached. Finally, the search algorithm searches in the opposite direction of the tip orientation vector by repeating all previous steps, then sorts all blobs in the clockwise or anti-clockwise direction.

II.C. Model based detection

After a list of catheter-like objects is found by one of the search algorithms, a cost function is used to estimate the likelihood of catheter-like objects. A generalized cost function was designed not only to discriminate the catheter from other radiographically dense objects, such as pacing leads and sternal wire loops, but also to recognize a catheter in a particular shape. It is defined as

$$\begin{aligned}
\text{Cost} = {} & w_0 * (1 - \text{Blob}_0) \\
& + w_1 * \frac{\sum_{i=1}^{N-1} |\text{Blob}_i - \overline{\text{Blob}}|}{N-1} \\
& + w_2 * \frac{\sum_{i=1}^{N-2} |\cos\beta_i - \overline{\cos\beta}|}{N-2} \\
& + w_3 * \frac{\text{ChordLen}}{\text{CurveLen}} \\
& + w_4 * (1.0 - e^{\frac{-(N-NE)^2}{NE^2}}) \\
& + w_5 * S_{\text{NCC}},
\end{aligned} \tag{7}$$

where w_i ($i = 0, \ldots, 5$) are weights that vary depending on the catheter type. Blob_i is the strength of the blob and Blob_0 is blob strength for the catheter tip. $\overline{\text{Blob}}$ is the mean blob strength of catheter electrodes excluding Blob_0. β is the folding angle and $\overline{\cos\beta}$ is the mean of cosines of all folding angles. ChordLen is the Euclidean distance between the last blob and Blob_0. CurveLen is the length of catheter (approximated by the line segments only). N is the number of blobs in the catheter-like object. *NE* is the expected number of

TABLE I. Weights of cost function for catheter detection.

Catheter	Training data size	w_0	w_1	w_2	w_3	w_4	w_5
CS	100	0.2	0.5	0.4	0.1	0.4	0
Ablation	100	0.4	0.1	0.4	0	0.3	0.6
Lasso (normal)	100	0.3	0.2	0	0.4	0.2	0
Lasso (line)	10	0.3	0	0.5	0	0.4	0

electrodes on the catheter. These could differ if closely spaced electrodes are detected as a single blob. Blob_i is normalized to a range of 0–1.0 over the 50 candidate blobs, so that if all weights are set to 1.0, all five parts of the equation have the same range from 0 to 1.0.

The first part of Eq. (7) penalizes a small tip electrode, as it should be one of the biggest blobs in the x-ray image. The second part is minimized when all electrodes (excluding the tip electrode) are equal size. The third part concerns the folding angle and penalizes sharp bends in the catheter. The fourth part is used to discriminate between open-curve shaped catheters and closed-curve shaped catheters. If ChordLen/CurveLen is applied to circular or elliptical shaped catheters (e.g., lasso catheter), it will generate a value near to zero. The fifth part is related to the number of electrodes on the catheter and it will reach zero when $N = NE$. Finally, S_{NCC} is a normalized template matching score and it calculates the normalized cross correlation between candidate catheter tip blob and a tip electrode template. This is used to detect different shapes of catheter tip electrodes.

For each type of catheter, certain parts of Eq. (7) are unnecessary, as detailed in Secs. II.C.1–II.C.4, and the weights are directly set to zero. Determining the best values for the remaining weights is an optimization problem and is solved separately for each catheter type using a brute-force approach of searching over all possible combinations of weights in the range 0.1–1.0 (step size 0.1) on a random set of training x-ray images. Since each training image may contain more than one catheter-like object, the lowest score is taken from each image at each combination of weights, and the optimized weights are those that give the minimum sum of these lowest scores. Table I gives the weights used for each type of catheter.

II.C.1. CS catheter detection

The CS catheter is an EP catheter inserted into the main branch of the coronary sinus tree. The most commonly used CS catheters are the ten-electrode or *decapolar* catheters. Once it is placed within the CS, the shape of the CS catheter is determined by the geometric shape of the CS main branch, which is a smoothly curving blood vessel. Therefore, the shape of the catheter is an open-end smooth curve and the smooth curve based search algorithm is used. w_5 was set to zero as the shape of the CS catheter tip electrode is similar to that of the lasso catheter.

II.C.2. Ablation catheter detection

The line based search algorithm was used for the ablation catheter, as it is very rigid in the region of the electrodes. In addition to the straight-line feature, the ablation catheter has a large and solid catheter tip electrode which casts a dark, solid, and thin ellipse-like blob in the x-ray images [see Fig. 5(a)]. A simple black template based on the estimated size was created in different orientations. The template is symmetric and orientations from 0° to 180° with a step of 1° were generated [see Fig. 5(b)]. Given a candidate tip blob, the template in the closest orientation with the first eigenvector of the tip blob is used. This template is translated along the first and second eigenvectors to find the optimal position by using a normalized cross correlation (NCC) algorithm.

As the template is symmetric and the catheter tip blob in the x-ray image is likely symmetric along the tip head and tip foot direction [see Fig. 5(c)], the first eigenvector and template matching cannot reliably distinguish the tip head where the ablation of heart muscle tissue takes place. Instead, this is determined from the direction of the remaining electrodes found in the two-direction line search. Part 3 of Eq. (7), $w_2 * \frac{\sum_{i=1}^{N-2} |\cos\beta_i - \overline{\cos\beta}|}{N-2}$, is replaced by $w_2 * (1 - \cos\theta)$. The turning angle θ [defined in Fig. 3(b)] is more robust than calculating the deviation of two folding angles. w_3 is set to zero, as the line shaped catheter is definitely an open-end curve (ChordLen/CurveLen is near the constant value of 1.0).

II.C.3. Lasso catheter detection

The physical shape of the lasso catheter is a closed circular curve [see Fig. 4(a)]. When it is perspectively projected onto

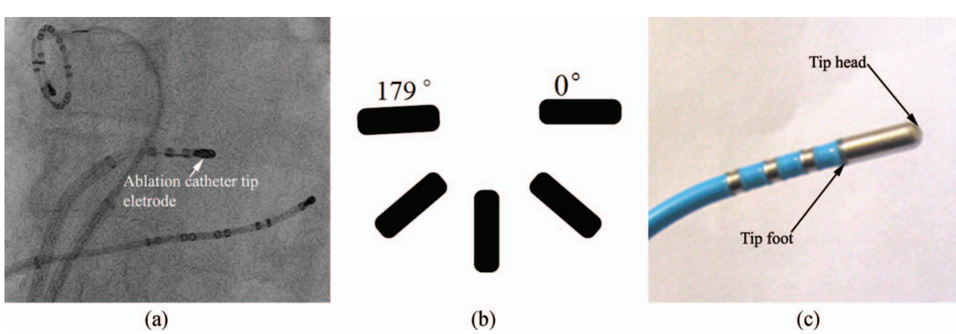

FIG. 5. (a) X-ray image of ablation catheter tip. (b) Ablation catheter tip templates in different orientations. (c) The definitions of the tip head and tip foot.

a 2D imaging plane by the x-ray system, the projected shape becomes a circle or an ellipse. The ellipse based search algorithm is therefore used to find the lasso catheter. In this case, w_2 is set to zero as folding angles are not reliable and there are always two sharp turns for elliptical objects. w_5 is also set to zero as the shape of the CS catheter tip electrode is similar to that of the lasso catheter.

Under some particular view orientations, the ellipse can collapse to a line segment. A line shaped lasso catheter can be found using the bidirectional line based search algorithm with a modified cost function similar to the ablation catheter cost function. Part 3 of Eq. (7), $w_2 * \frac{\sum_{i=1}^{N-2} |\cos\beta_i - \overline{\cos\beta}|}{N-2}$, is again replaced by $w_2 * (1 - \cos\theta)$, where the angle θ is defined in this case as the angle between the orientation vector and the line vector determined by least-squares fitting. In the current implementation, the switch between elliptical shape detection and line shape detection is manual.

II.C.4. Simultaneous detection

In some clinical applications, the ablation catheter, lasso catheter, and CS catheter are required to be detected simultaneously as the ablation catheter detection can localize the 3D position of the catheter tip and the lasso catheter or CS catheter can be used for motion correction or motion gating. Therefore, a framework of detecting these three catheters simultaneously was developed.

Figure 6 presents the flow chart for this framework. The preprocessing steps are to estimate the magnification factor of the x-ray system then generate the tip templates for the ablation catheter. This is followed by blob detection and eigenvector calculation. From the blob data, the CS catheter is detected first. The ablation and finally the lasso catheter are then detected using the remaining blobs and their eigenvectors. The order of catheter detection is determined by the robustness of detecting each catheter. The CS catheter detection is most robust, as this catheter comprises a long smooth curve with no self-occlusion. The ablation catheter is then easily detected by its distinctive tip electrode, leaving the lasso catheter to be detected from a reduced number of candidate blobs.

II.D. Template-based tracking

If the x-ray view does not change, catheter tracking methods can be used to increase the robustness of the catheter detection method. Tracking methods are initialised using the basic detection algorithm described in Sec. II.C. This detection is used to create a customized 2D catheter model comprising a connected graph which gives information about the initial shape and orientation of the catheter. In subsequent frames, the tracking methods use the same blob detection method and a modified catheter detection method that uses the customized model. Incorporating the customized model may allow successful tracking in cases where some catheter electrodes are overlapped with other radiographically dense objects or are outside the field of view. The current implementation requires manual detection of failed tracking, at which point the operator can restart with the basic detection algorithm.

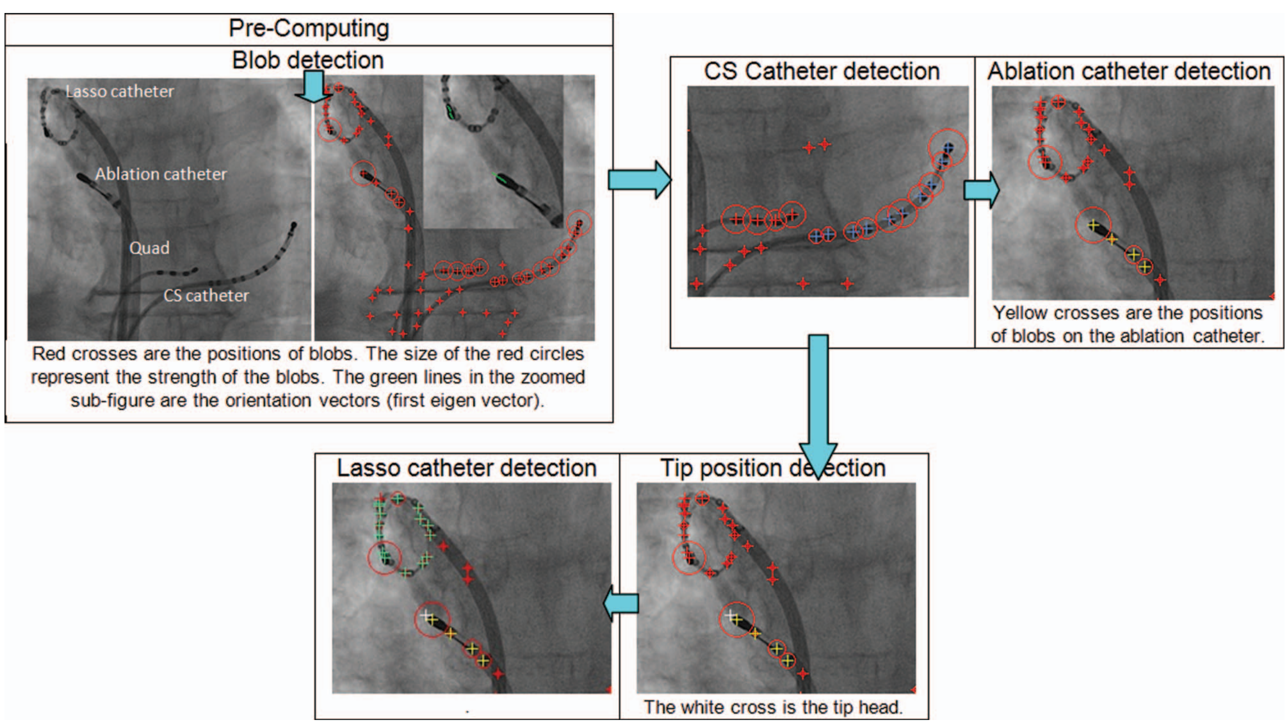

FIG. 6. The flow chart of simultaneous catheter detection. The detection method starts with blob detection and eigenvector calculation. The CS catheter is detected first using the result of blob detection only. The ablation and lasso catheters are then detected using the results of blob detection and eigenvector calculation.

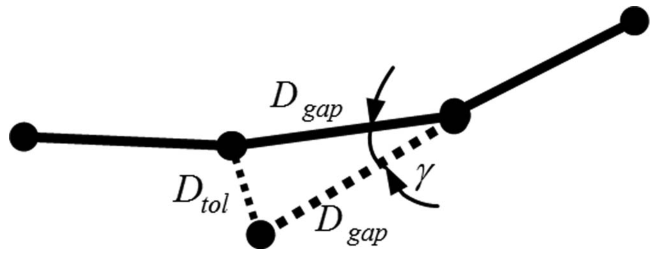

FIG. 7. The definition of D_{tol} and γ.

II.D.1. CS catheter tracking

The customized model for the CS catheter comprises the orientation vector of the catheter tip and the positions of the electrode blobs. The search algorithm assumes that the catheter tip electrode (the distal electrode) is not overlapped. It again starts with the first ten strongest blobs and uses them as the candidates for the catheter tip electrode. The customized model is aligned with each candidate for the catheter tip electrode and rotated within the image plane to match the direction of the catheter tip orientation vector (determined from the first eigenvector of the tip electrode and the direction vector between the first two electrodes). From the position of the tip electrode, the search algorithm finds all blobs which are within the maximum gap distance, D_{gap}, between the candidate blob and catheter tip blob. D_{gap} is the maximum gap between any two electrodes in the customized model. If the minimum distance from the candidate blobs to the catheter tip blob is less than the tolerance distance, D_{tol}, then the candidate blob with the minimum distance will be chosen. Otherwise, the electrode is likely overlapped by other radiographically dense objects and is undetected. The corresponding electrode in the customized model will then be chosen instead. The tolerance distance, D_{tol}, is defined as $D_{\mathrm{tol}} = 2\sin(\gamma/2)D_{\mathrm{gap}}$. γ is the maximum deformation angle and is related to the local deformation of the CS catheter (see Fig. 7). From the observation of all our x-ray images, $\gamma < 30^\circ$. Therefore, $D_{\mathrm{tol}} = 0.518D_{\mathrm{gap}}$ is chosen.

The search algorithm will continue searching through the candidate blobs until the number of selected blobs is equal to the number of electrodes in the customized model or no more blobs can be found within D_{gap}. After the search algorithm obtains one or several candidate catheter objects, the same cost function with the same weights as the one used in detection is used to select the best CS catheter candidate.

The tracking method can also deal with partially missing data, which is caused by some electrodes occasionally moving outside the field of view. This may be caused by significant cardiac or respiratory motion, the degree of x-ray magnification or the amount of collimation. For missing proximal-end electrodes, the number of electrodes compulsory for matching the customized CS catheter model is relaxed. For missing distal-end electrodes, the blobs near the boundary of the image are used as the catheter tip blob and the search algorithm starts from this. Currently, the choice of which of these methods to apply must be determined manually.

II.D.2. Ablation catheter tracking

For the ablation catheter, the model again comprises the orientation vector of the catheter tip and the positions of all electrodes. Similar to the CS catheter tracking, the search algorithm first aligns the position and the orientation vector of the catheter tip electrode and then matches the other three electrodes.

II.D.3. Lasso catheter tracking

As opposed to the CS and ablation catheters, the order of electrodes in the lasso catheter is not reliable, due to the self-overlapping electrodes. Therefore, the search algorithm can only match the catheter tip and use the customized shape model (ellipse, circle, or line) to match the remaining part of the catheter. To generate the customized shape model, the least squares fitting algorithm is used to fit an ellipse to the electrode positions. This refined shape model is used to constrain the search for the candidate blobs by minimizing the distance between the blob position and the shape model.

III. RESULTS

Clinical x-ray images, 2292, (excluding 310 images used for training to determine weights) were used to test the three proposed catheter detection and tracking methods. There were a total of 105 different clinical fluoroscopy sequences which came from 31 atrial fibrillation (AF) ablation clinical cases. Typically, the clinical x-ray images contained one CS catheter, one ablation catheter, and sometimes one lasso catheter. All 2292 images were used for testing CS catheter detection and tracking, 2014 images for the ablation catheter, and 1677 images for the lasso catheter. The same 1677 images were used to test the simultaneous detection and tracking, as they contained all three catheters. Not all images were used for the ablation or lasso catheter, as these were not visible in all the x-ray images.

To measure detection and tracking accuracy, two clinical experts manually picked the center position of each electrode on all 2292 images. The 2D distance between the manually defined positions and the positions detected by the detection or tracking method were measured, at the x-ray detector scale. Mean and standard deviation errors were calculated for each catheter using all available images and considering the normal and low dose images separately. A failed detection for a catheter was defined as one where any of the electrodes on that catheter had an error of more than 2 mm. This was used to calculate the overall success rate of the detection or tracking. Frame rate was determined using a single-threaded CPU implementation on an Intel Core 2 Duo 2.0 GHz laptop with an nVidia Quadro FX 350M graphics card. Table II summarizes detection and tracking results for each catheter in terms of error, success rate, and frame rate. Figure 8 shows statistics of the error for each electrode separately. Root mean square (RMS) deviations were used to measure the interobserver variability between the two observers. The measurement was the RMS error distances between the points marked by the first observer and the second observer. Results show a

TABLE II. Results for catheter detection and tracking methods on individual catheters.

	Catheter	CS	Ablation	Lasso
Detection	Error for all images (mm)	0.50 ± 0.29	0.92 ± 0.61	0.63 ± 0.45
	Error for low dose (mm)	0.49 ± 0.27	0.96 ± 0.63	0.61 ± 0.43
	Success rate (%)	99.4	97.2	88.9
	Frame rate (fps)	21	15	17
Tracking	Error for all images (mm)	0.45 ± 0.28	0.64 ± 0.37	0.53 ± 0.38
	Error for low dose (mm)	0.44 ± 0.28	0.67 ± 0.39	0.52 ± 0.34
	Success rate (%)	100	99.2	96.5
	Frame rate (fps)	23	17	20

difference of 0.12 mm for normal dose images (940 images) and 0.14 mm for low dose images (1352 images). There was no significant difference between the two observers.

Three experienced electrophysiologists carried out an evaluation of the catheter detection and tracking in terms of potential clinical utility. They were asked to score the results of CS, ablation, lasso and simultaneous catheter tracking after viewing videos of the tracking results in each sequence. The videos showed the original x-ray sequence and annotated electrode positions on the catheters. Each clinical expert was instructed to score videos according to Table III. There were 58 videos, each showing tracking of CS, ablation, and lasso catheters. The average results of the scoring were 4.1 for CS, 4.2 for ablation, 3.7 for lasso, and 4.0 for simultaneous tracking. To determine the interobserver variability, the p-values of t-tests were calculated for all pairs of observers and for all types of tracking method. The minimum of the p-values was 0.25, which indicates that there were no significant interobserver differences.

For the CS catheter, it is noticeable that electrode no. 2 has relatively larger errors than the others. This is because the second electrode is very close to the catheter tip (the distal electrode) and it could be detected together with the catheter tip as a single large blob. The detection method was robust

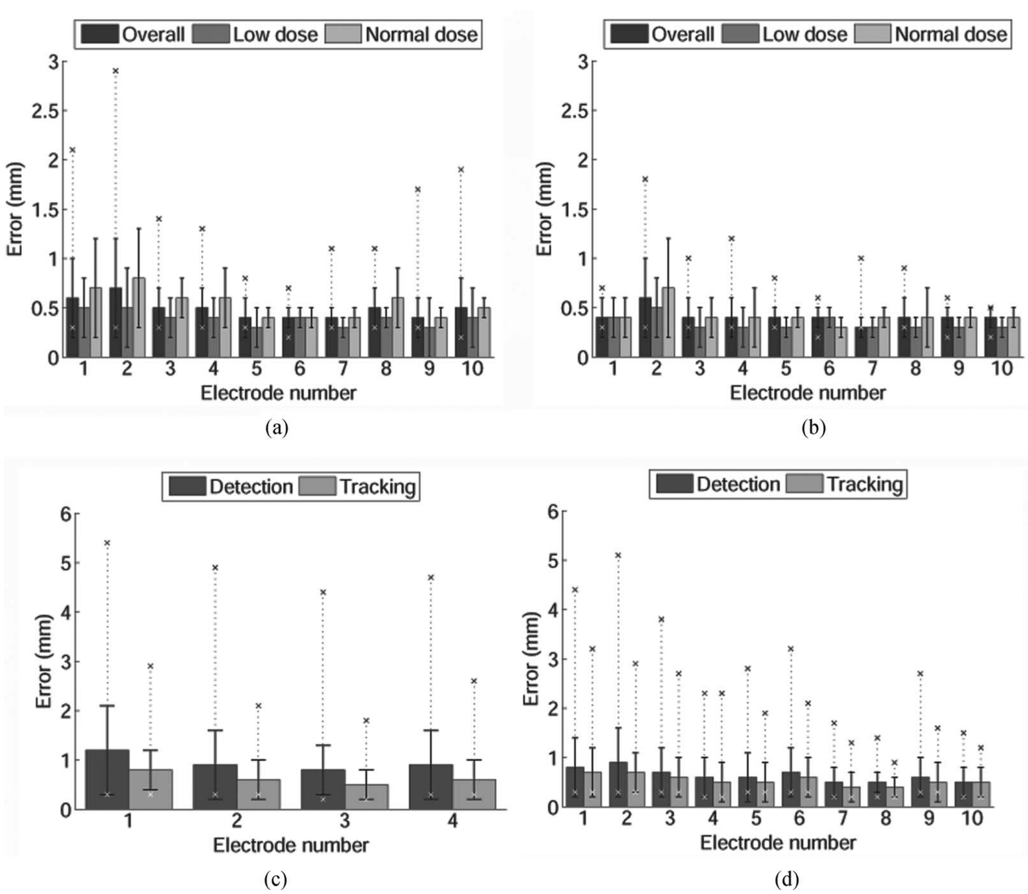

FIG. 8. 2D detection and tracking errors for individual catheters. (Catheter tip is electrode no. 1). The height of the solid bar is the mean error. The error bar shows the standard deviation. The black cross is the maximum error and white cross is the minimum error. Only the first ten electrodes are shown for the lasso catheter. (a) CS detection results. (b) CS tracking results. (c) Ablation catheter results. (d) Lasso catheter results.

TABLE III. Meaning of score for subjective clinical evaluation. Minimal manual intervention would mean reinitialization of the detection and tracking. Significant manual intervention would mean manual identification of catheters by mouse click followed by reinitialization of detection and tracking.

Score	Meaning
5	(i) All catheters and electrodes identified correctly; (ii) no observable errors
4	As per (i) above but (ii) a few frames have electrode annotation errors that would not affect clinical utility
3	As per (i) above but (ii) a few frames have electrode annotation errors that would compromise clinical utility but manual intervention not required
2	As per (i) above but (ii) a few frames have electrode annotation errors that would compromise clinical utility and minimal manual intervention required
1	(i) Electrodes annotated on wrong objects; (ii) significant manual intervention required
0	(i) At least one catheter not annotated; (ii) significant manual intervention required

TABLE IV. Results for simultaneous catheter detection and tracking methods.

	Catheter	CS	Ablation	Lasso
Detection	Error (mm)	0.48 ± 0.31	0.81 ± 0.59	0.61 ± 0.44
	Success rate (%)		89.5	
	Frame rate (fps)		16	
Tracking	Error (mm)	0.42 ± 0.25	0.63 ± 0.38	0.51 ± 0.32
	Success rate (%)		97.8	
	Frame rate (fps)		18	

for low dose images and the errors were very similar to those for normal dose images. There was failure of detection in 14 frames of normal dose images because one of the electrodes was occluded by ECG electrodes. The tracking method had similar accuracy. Furthermore, the tracking method correctly tracked all electrodes in the 14 frames of x-ray images where the detection method failed. The ablation detection and tracking methods achieved similar success rates to the

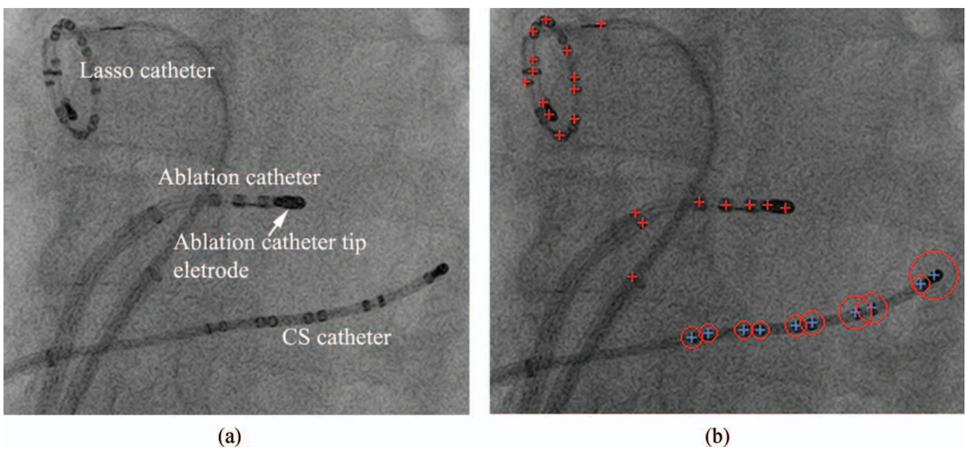

FIG. 9. Example of CS catheter detection in a low dose X-ray image. (a) Original low dose X-ray image. (b) CS catheter detection result. The crosses on the CS catheter are the positions of CS catheter electrodes. All other crosses are the positions of other catheter electrodes. The size of the circles on the catheter represent the strength of the blobs.

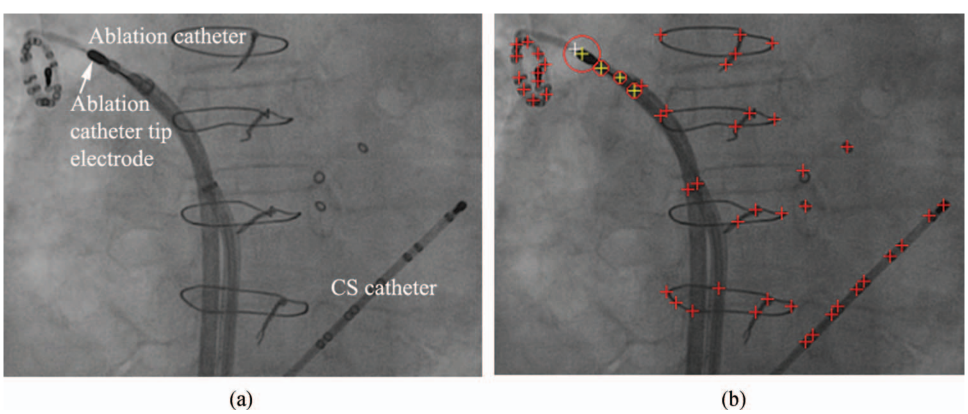

FIG. 10. Example of ablation catheter detection in a normal dose X-ray image. (a) Original X-ray image. (b) Ablation catheter detection result. The crosses on the ablation catheter are the positions of ablation catheter electrodes. The white cross is the position of the ablation catheter tip electrode, where the ablation of heart muscle tissue takes place. The other crosses are the positions of other objects. The size of the circles represent the strength of the blobs (enhanced online) [URL: http://dx.doi.org/10.1118/1.4808114.1].

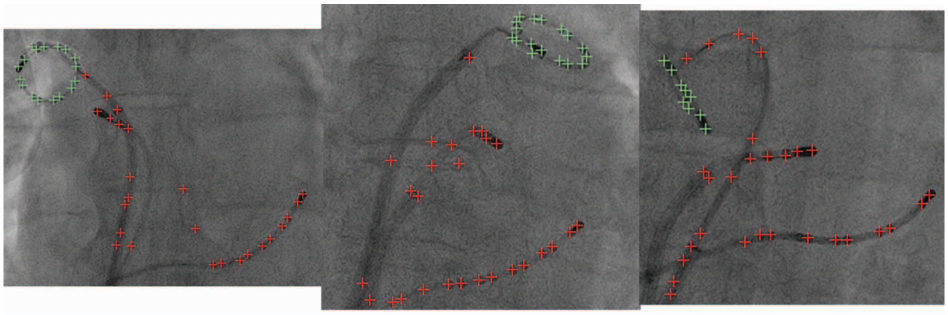

FIG. 11. Examples of lasso catheter detection in low dose X-ray images. The crosses on the lasso catheter are the positions of blobs on the lasso catheter. The other crosses are the positions of other objects. (a) Ellipse shape. (b) Thin ellipse shape. (c) Line shape (enhanced online) [URL: http://dx.doi.org/10.1118/1.4808114.2].

FIG. 12. Example of simultaneous catheter detection in a low dose X-ray image. The crosses on the lasso catheter, the crosses on the ablation catheter and the crosses on the CS catheter are the positions of blobs on the lasso catheter, ablation catheter and CS catheter, respectively. The other crosses are the positions of other objects (enhanced online) [URL: http://dx.doi.org/10.1118/1.4808114.3].

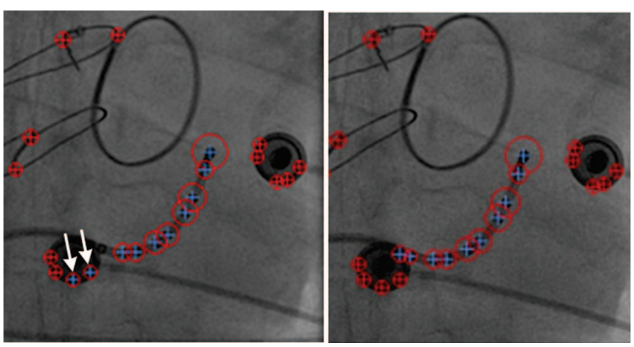

FIG. 13. Examples of CS catheter tracking vs. catheter detection. The crosses on CS catheter are the catheter electrodes. The other crosses are other objects. The left image is the result of catheter detection (arrows show failed detection of the last two electrodes) and the right image is the result of catheter tracking. Note that the CS catheter in the right image is correctly identified.

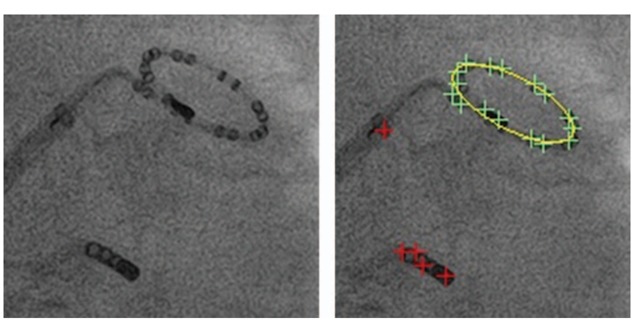

FIG. 14. The least squares fitting of an ellipse for the lasso catheter.

CS methods, but are slightly slower due to the additional computational cost of the NCC algorithm. For the lasso catheter, the detection success rate is lower than for the other catheters. The majority of these failures are caused by overlapping with the ablation catheter, which leads to some of the electrodes having higher detection errors. The tracking method avoids most of the failures and has a success rate comparable to the other catheters. For the simultaneous method, the detection and tracking results are given in Table IV. Success was defined as all three types of catheter being detected successfully.

Figures 9–12 show examples of detection for each type of catheter and for simultaneous detection. Figures 13 and 14 are examples of tracking. Figure 13 is a case of CS catheter tracking where the detection method fails to locate two of the electrodes due to occlusion, but locates the electrodes using the tracking method. This demonstrates the value of the tracking algorithm for tracking catheters that are partially occluded or out of view. Figure 14 demonstrates lasso catheter tracking using a parametric ellipse model.

IV. DISCUSSION AND CONCLUSIONS

This paper presents and validates a novel and real-time image-based catheter detection framework for EP procedures. The proposed detection and tracking methods are automatic, but currently require user interaction to detect failures and restart the detection in these cases. The methods can detect CS, ablation, and lasso catheters simultaneously and in real-time. The accuracy of the proposed methods is sub-mm and the methods are robust towards low-dose x-ray fluoroscopic images, which are mainly used during EP procedures to maintain low radiation dose. The developed catheter detection algorithms were able to automatically recognize catheter-like objects to a high degree of robustness. Customized shape models were extracted from the detection methods and these shape models were used as input for tracking algorithms that improved the robustness further. The use of the customized shape models was important to reduce failed detections when catheter electrodes were overlapped by other structures or when catheter electrodes were partially outside the field of view.

Higher errors in ablation catheter detection or tracking are caused by detection or tracking the wrong object which is far away from the real ablation catheter. The templates of the ablation catheter tip electrodes were created assuming that the tip electrode was laying flat on the x-ray image plane. However, because we also take account of the blob size (tip size on the image) and the shape of catheter (straight line), the tracking/detection algorithm was generally robust towards the situation when the tip head was positioned to face the user. The higher failure rate and lower errors (compared with the ablation catheter) of the lasso catheter are caused by overlapping with the ablation catheter. In the overlapping cases, some of the electrodes on the ablation catheter were detected as the electrodes on the lasso catheter. Although the success rate of detection and tracking are high (from 89% to 100%), some failure cases may happen during clinical procedures and these currently need manual intervention to detect the failure and restart the detection. The results of the clinical evaluation study demonstrate that such manual intervention would be uncommon.

Previously published methods have reported an accuracy of 0.76 mm mean error and 97.8% success rate for CS catheter detection[25] and a detection failure rate of 3.97% for multiple catheters.[26] In comparison our tracking method is more accurate (0.45 ± 0.28 mm) and more robust (100% success rate) for CS catheters, and similarly robust for multiple catheters (97.8% success rate with a wider success threshold). Our method is also faster than previously reported frame rates, achieving a constant speed of 23 fps for CS catheter tracking and 18 fps for simultaneous tracking, evaluated on a low speed laptop, compared to 5 fps (Ref. 25) and 10 fps.[26] The limitation of our method compared to these approaches is that it assumes a desired or fixed shape for the catheter and might not cope with the catheter changing shape or the C-arm being positioned at an extreme angle.

As the proposed methods use blob detection to extract the key information from the whole x-ray image, the computational cost of detecting a catheter from the extracted information is relatively low compared with methods based on the vessel-filtering approach.[13] The proposed computational framework is not limited to detect only CS, ablation, and lasso catheters and it could be extended to any EP catheters as long as a shape model can be built and physical measurements can be obtained. The CS catheter detection examples shown in this paper are for detecting ten-electrode CS catheters but the method could be applied to other types of CS catheters such as 4-electrode, 7-electrode, or 12-electrode measurement catheters. The methods could also be applied to pacing leads for cardiac resynchronization therapy. A limitation of the techniques is that only electrodes are detected and the rest of the catheter is not detected or tracked. However, for the majority of EP clinical applications, the position of the electrodes is most important.

The very high robustness achieved when using a combination of detection and tracking will be important when translating these algorithms into clinically useful tools. There is a wide range of potential applications. One important application is respiratory motion correction for 3D anatomical overlay guided EP interventions.[4] As both the CS catheter and lasso catheter can be reliably tracked, they can be used to correct the respiratory motion. Another application is automatic image-based ablation point localization.[18]

In conclusion, a robust and accurate framework is presented for the detection of the three most common types of EP catheters without user interaction. The framework allows detection of individual catheters or a combination of catheters with robustness to low dose x-ray images, overlapping structures, and partially missing catheter structures. The proposed approach has potential utility in EP procedures for annotating catheter position and correcting for patient motion when used in conjunction with anatomical overlays.

ACKNOWLEDGMENTS

This work was supported by funding from Philips Healthcare, Best, The Netherlands, and the KCL Centre of Excellence in Medical Engineering funded by the Wellcome Trust and the EPSRC under Grant No. WT 088641/Z/09/Z. Support was also provided by the National Institute for Health Research (NIHR) Biomedical Research Centre at Guy's and St Thomas' NHS Foundation Trust and King's College London. The views expressed are those of the authors and not necessarily those of the NHS, the NIHR, or the Department of Health.

[a] Author to whom correspondence should be addressed. Electronic mail: y.ma@kcl.ac.uk

1. J. Ector, S. De Buck, W. Huybrechts, D. Nuyens, S. Dymarkowski, J. Bogaert, F. Maes, and H. Heidbüchel, "Biplane three-dimensional augmented fluoroscopy as single navigation tool for ablation of atrial fibrillation: Accuracy and clinical value," Heart Rhythm **5**, 957–964 (2008).
2. S. Knecht, H. Skali, M. D. O'Neill, M. Wright, S. Matsuo, G. Chaudhry, C. Haffajee, I. Nault, G. Gijsbers, F. Sacher, F. Laurent, M. Montaudon, O. Corneloup, M. Hocini, M. Haïssaguerre, M. Orlov, and P. Jaïs, "Computed tomography-fluoroscopy overlay evaluation during catheter ablation of left atrial arrhythmia," Europace **10**, 931–938 (2008).
3. J. Sra, G. Narayan, D. Krum, A. Malloy, R. Cooley, A. Bhatia, A. Dhala, Z. Blanck, V. Nangia, and M. Akhtar, "Computed tomography-fluoroscopy image integration-guided catheter ablation of atrial fibrillation," J. Cardiovasc. Electrophysiol. **18**, 409–414 (2007).
4. K. S. Rhode, M. Sermesant, D. Brogan, S. Hegde, J. Hipwell, P. Lambiase, E. Rosenthal, C. Bucknall, S. A. Qureshi, J. S. Gill, R. Razavi, and D. L. G. Hill, "A system for real-time XMR guided cardiovascular intervention," IEEE Trans. Med. Imaging **24**, 1428–1440 (2005).
5. M. Orlov, P. Hoffmeister, G. Chaudhry, I. Almasry, G. Gijsbers, T. Swack, and C. Haffajee, "Three-dimensional rotational angiography of the left atrium and esophagus: A virtual computed tomography scan in the electrophysiology lab," Heart Rhythm **4**, 37–43 (2007).
6. A. Al-Ahmad, L. Wigström, D. Sandner-Porkristl, P. Wang, P. Zei, J. Boese, G. Lauritsch, T. Moore, F. Chan, and R. Fahrig, "Three-dimensional rotational angiography of the left atrium and esophagus: A virtual computed tomography scan in the electrophysiology lab," Heart Rhythm **5**, 513–519 (2008).
7. G. Nolker, K. Gutleben, H. Marschang, G. Ritscher, S. Asbach, N. Marrouch, J. Brachmann, and A. Sinha, "Three-dimensional left atrial and esophagus reconstruction using cardiac C-arm computed tomography with image integration into fluoroscopic views for ablation of atrial fibrillation: Accuracy of a novel modality in comparison with multislice computed tomography," Heart Rhythm **5**, 1651–1657 (2008).
8. Y. Ma, G. P. Penney, D. Bos, P. Frissen, C. Rinaldi, R. Razavi, and K. Rhode, "Hybrid echo and X-ray image guidance for cardiac catheterization procedures by using a robotic arm: a feasibility study," Phys. Med. Biol. **55**, N371–N382 (2010).

[9]G. Gao, G. Penney, Y. Ma, N. Gogin, P. Cathier, A. Arujuna, G. Morton, D. Caulfield, J. Gill, C. A. Rinaldi, J. Hancock, S. Redwood, M. Thomas, R. Razavi, G. Gijsbers, and K. Rhode, "Registration of 3D trans-esophageal echocardiography to X-ray fluoroscopy using image-based probe tracking," Med. Image Anal. **16**, 38–49 (2012).

[10]K. Rhode and M. Sermesant, "Modeling and registration for electrophysiology procedures based on three-dimensional imaging," Curr. Cardiovasc. Imaging Rep. **4**, 116–126 (2011).

[11]S. Huang and M. Wood, *Catheter Ablation of Cardiac Arrhythmias*, 2nd ed. (Saunders, Texas, 2010).

[12]A. King, R. Boubertakh, K. Rhode, Y. Ma, P. Chinchapatnam, G. Gao, T. Tangcharoen, M. Ginks, M. Cooklin, J. Gill, D. Hawkes, R. Razavi, and T. Schaeffter, "A subject-specific technique for respiratory motion correction in image-guided cardiac catheterisation procedures," Med. Image Anal. **13**, 419–431 (2009).

[13]A. Brost, R. Liao, J. Hornegger, and N. Strobel, "3-D respiratory motion compensation during EP procedures by image-based 3-D lasso catheter model generation and tracking," in *Medical Image Computing and Computer-Assisted Intervention-MICCAI*, Lecture Notes in Computer Science Vol. 5761 (Springer, London, U.K., 2009) pp. 394–401.

[14]A. Brost, R. Liao, J. Hornegger, and N. Strobel, "Respiratory motion compensation by model-based catheter tracking during EP procedures," Med. Image Anal. **14**, 695–706 (2010).

[15]Y. L. Ma, A. P. King, N. Gogin, C. A. Rinaldi, J. Gill, R. Razavi, and K. Rhode, "Real-time respiratory motion correction for cardiac electrophysiology procedures using image-based coronary sinus catheter tracking," in *Medical Image Computing and Computer-Assisted Intervention-MICCAI*, Lecture Notes in Computer Science Vol. 6361 (Springer, Beijing, China, 2010), pp. 391–399.

[16]Y. L. Ma, A. P. King, N. Gogin, G. Gijsbers, C. A. Rinaldi, J. Gill, R. Razavi, and K. Rhode, "Comparing image-based respiratory motion correction methods for anatomical roadmap guided cardiac electrophysiology procedures," in *Functional Imaging and Modeling of the Heart-FIMH*, Lecture Notes in Computer Science Vol. 6666 (Springer, New York, NY, 2011), pp. 55–62.

[17]Y. Ma, A. King, N. Gogin, G. Gijsbers, C. A. Rinaldi, J. Gill, R. Razavi, and K. Rhode, "Clinical evaluation of respiratory motion compensation for anatomical roadmap guided cardiac electrophysiology procedures," IEEE Trans. Biomed. Eng. **59**, 122–131 (2012).

[18]Y. L. Ma, G. Gao, G. Gijsbers, C. A. Rinaldi, J. Gill, R. Razavi, and K. Rhode, "Image-based automatic ablation point tagging system with motion correction for cardiac ablation procedures," in *Information Processing in Computer-Assisted Interventions*, Lecture Notes in Computer Science Vol. 6689 (Springer, Berlin, Germany, 2011), pp. 145–155.

[19]H. J. Bender, R. Männer, C. Poliwoda, S. Roth, and M. Walz, "Reconstruction of 3D catheter paths from 2D X-ray projections," in *Medical Image Computing and Computer-Assisted Intervention*, Lecture Notes in Computer Science Vol. 1679 (Springer, London, U.K., 1999), pp. 981–989.

[20]P. Fallavollita, "2D/3D registration of mapping catheter images for arrhythmia interventional assistance," Int. J. Comput. Sci. Issues **4**, 10–19 (2009).

[21]H. Sundar, A. Khamene, L. Yayziv, and C. Xu, "Automatic image-based cardiac and respiratory cycle synchronization and gating of image sequences," in *Medical Image Computing and Computer-Assisted Intervention-MICCAI*, Lecture Notes in Computer Science Vol. 5762 (Springer, London, U.K., 2009), pp. 381–388.

[22]E. Franken, P. Rongen, M. Almsick, and B. Romeny, "Detection of electrophysiology catheters in noisy fluoroscopy images," in *Medical Image Computing and Computer-Assisted Intervention-MICCAI*, Lecture Notes in Computer Science Vol. 4191 (Springer, Copenhagen, Denmark, 2006), pp. 25–32.

[23]R. van der Weide, C. Bakker, and M. Viergever, "Localization of intravascular devices with paramagnetic markers in mr images," IEEE Trans. Med. Imaging **20**, 1061–1071 (2001).

[24]M. Schenderlein, S. Stierlin, R. Manzke, V. Rasche, and K. Dietmayer, "Catheter tracking in asynchronous biplane fluoroscopy images by 3D B-snakes," Proc. SPIE **7625**, 1097–1104 (2010).

[25]W. Wu, T. Chen, A. Barbu, P. Wang, N. Strobel, S. Zhou, and D. Comaniciu, "Learning-based hypothesis fusion for robust catheter tracking in 2D X-ray fluoroscopy," in *Proceeedings of Conference on Computer Vision and Pattern Recognition, Colorado* (IEEE, Colorado, 2011), pp. 1097–1104.

[26]L. Yatziv, M. Chartouni, S. Datta, and G. Sapiro, "Toward multiple catheters detection in fluoroscopic image guided interventions," IEEE Trans. Inf. Technol. Biomed. **16**, 770–781 (2012).

[27]T. Lindeberg, "Detecting salient blob-like image structures and their scales with a scale-space primal sketch: A method for focus-of-attention," Int. J. Comput. Vis. **11**, 283–318 (1993).

[28]T. Lindeberg, "Scale-space," *Encyclopedia of Computer Science and Engineering* (John Wiley and Sons, Urbana, 2009), pp. 2495–2540.